# Diffusion-Mediated Superelongation in Metal Nanorods

Hui Fang,[1,†] Yangyang Pan,[1,†] Bozhao Wu,[1] Cai Lu,[1] Wengen Ouyang,[1,2] and Ze Liu[1,2,3,*]
[1]Department of Engineering Mechanics, School of Civil Engineering, Wuhan University, Wuhan, 430072, China
[2]State Key Laboratory of Water Resources Engineering and Management, Wuhan University, Wuhan, Hubei, 430072, China
[3]The Institute of Technological Sciences, Wuhan University, Wuhan, 430072, China

(Received 10 August 2023; revised 17 January 2024; accepted 25 April 2024; published 17 June 2024)

We report *in situ* electron microscopy observation of the superelongation deformation of low-melting-point metal nanorods. Specifically, metal nanorods with diameters as small as 143 nm can undergo uniform stretching by an extraordinary 786% at $\sim 0.87T_m$ without necking. Moreover, the corresponding fracture stress exhibits a pronounced size effect. By combining experimental observations with molecular dynamic simulations, a crystal-core–liquid-shell structure is revealed, based on which a constitutive model that incorporates diffusion creep mechanism and surface tension effect is developed to rationalize the findings. This study not only establishes a pioneering reference for comprehending the diffusion-dominated constitutive response of nanoscale materials but also has substantial implications for strategic design and processing of metals in high-temperature applications.

DOI: 10.1103/PhysRevLett.132.256201

The size effect in mechanical deformation has been studied intensively and well exploited for industrial use after the pioneering *in situ* nanoindentation experiments by Uchic *et al.* [1], but mainly limited to room temperature condition. Creep, the time-dependent deformation at elevated temperatures, is a crucial concern in engineering applications [2]. Atomic diffusion forms a fundamental mechanism in creep, however, its direct experimental linkage to macroscopic mechanical behavior poses a significant challenge. The Nabarro [3] and Herring [4] models quantitatively depict crystal deformation under elevated temperature and at low-stress conditions. These models consider the influence of nonhydrostatic stress fields, leading to vacancy concentration gradients within crystals and consequent matter transport. Subsequently, Coble [5] proposed a creep mechanism controlled by grain-boundary diffusion, recognizing that the grain-boundary diffusion can surpass self-diffusion within grains at temperatures lower than $0.7T_m$. Diffusion creep is of great significance in many fields [6,7], including nuclear energy [8], superplasticity [9–11], friction [12–14], sintering [15–18], lithium dendrization [19,20], and geoscience [21]. Despite its importance, the confirmation of diffusional creep has primarily relied on indirect experimental evidence. Recent advancements in high-resolution electron microscopy have shed light on the deformation mechanisms of nanosized silver samples (with sizes below ~10 nm). These investigations have underscored the dominant role of surface diffusion, giving rise to the "smaller is much weaker" phenomenon [13,22,23]. *In situ* experimental visualization has provided evidence of the diffusion-assisted dislocation nucleation process [24], further supporting this concept. Notably, *in situ* nanomechanical testing is typically conducted at room temperature due to the challenge in achieving temperature uniformity at nanoscale [25,26]. At relatively low temperatures, multiple mechanisms such as diffusion creep, dislocation creep, and grain-boundary sliding, can collectively contribute to the material behaviour [24]. Hence, obtaining direct experimental evidence of diffusion creep and establishing a direct connection between the atomic-scale matter transport and its constitutive response continue to present a significant challenge.

Considering the unique insight offered by the free surface of nanosized sample into matter transport during deformation [24], we employ the superplastic nanomolding technique [27,28] to fabricate metal nanorods with low melting point at room temperature. Subsequently, *in situ* tensile testing of the fabricated nanorods is performed under scanning electron microscopy [29] to investigate their plastic response driven by diffusion. The surface matter transport during superelongation deformation of metal nanorods is directly captured. A crystal-core–liquid-shell structure is then proposed to rationalize the findings based on TEM characterization and molecular dynamics (MD) simulations. Furthermore, we develop a physical mechanism-based constitutive model that integrates the atomic diffusion mechanism and the surface tension effect, which can well reproduce the "rubberlike" superelongation deformation of metal nanostructures nearby their melting temperature.

To underline the diffusion creep, we selected a low-melting-point alloy (InBiSn with $T_m \sim 334$ K, Fig. S1 [30]) for nanomolding at room temperature [27,28] [Figs. 1(a) and 1(b)]. Previous studies have shown that if superplastic nanomolding is performed at the diffusion deformation-dominated temperature range (typically $T \geq 0.5T_m$),

 

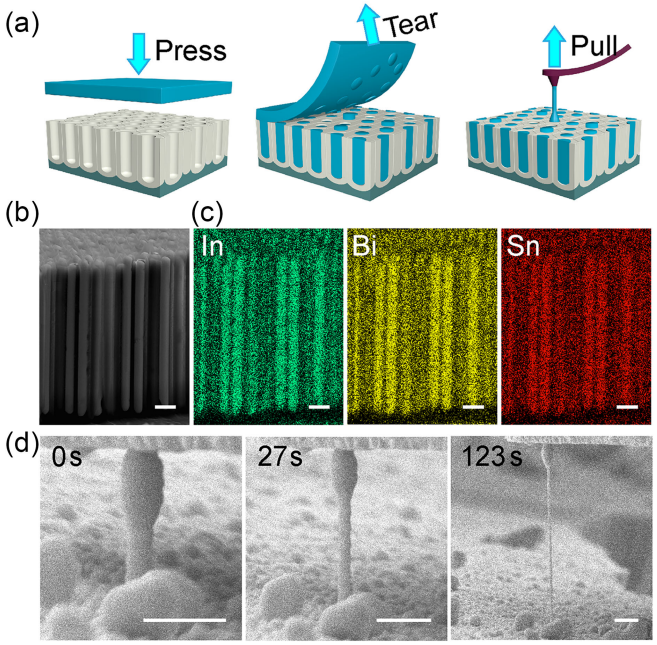


FIG. 1. "Rubberlike" superelongation of metal nanorods. (a) Schematic of the experimental setup. A low-melting-point metal is first compressed into a hard mold with cylindrical nanocavities. Subsequently, the molded metal nanorods are exposed by mechanically peeling off the substrate. Finally, tensile of metal nanorods is achieved by adhering a probe to the top of an exposed nanorod and then controlled moving the probe (see Supplemental Material [30]). (b) Sectional view of typical fabricated InBiSn nanorods by intentionally breaking the molded sample. Scale bar: 800 nm. (c) EDS maps of the InBiSn nanorods. Scale bars: 800 nm. (d) Selected frames from the video of *in-situ* tensile of an InBiSn nanorod (see Supplemental Material, Movie 1). Scale bars: 400 nm.

molded metal or alloy nanostructures will exhibit great crystallinity [27,36,37]. The uniform distribution of components was subsequently verified by energy-dispersive x-ray spectroscopy (EDS) mapping the molded InBiSn nanorods [Fig. 1(c)]. During a typical *in situ* tensile of a molded InBiSn nanorod at room temperature (~20 °C), we observed a uniform superelongation (~786%) of the InBiSn nanorod [Fig. 1(d)], without noticeable necking prior to fracture. Similar behavior was also observed during the tensile of In nanorods at room temperature (~$0.68T_{\mathrm{m}}$, Supplemental Material, Movie 2 [30]).

We further employed a force probe with a spring constant of ~35 N/m (FMT-120, Klendick) to monitor the tensile force during stretching. Typical results are shown in Fig. 2. Dividing the tensile force by the cross-sectional area of the stretched InBiSn nanorod gives the stretching stress, which first increases slowly with the stretch ratio and then shots up [red dots in Fig. 2(a)]. This behavior closely resembles the hyperelastic deformation observed in rubberlike materials. The difference is that the superelongation here originates from diffusion-based plastic deformation. The evidence can be found in the relationship between the

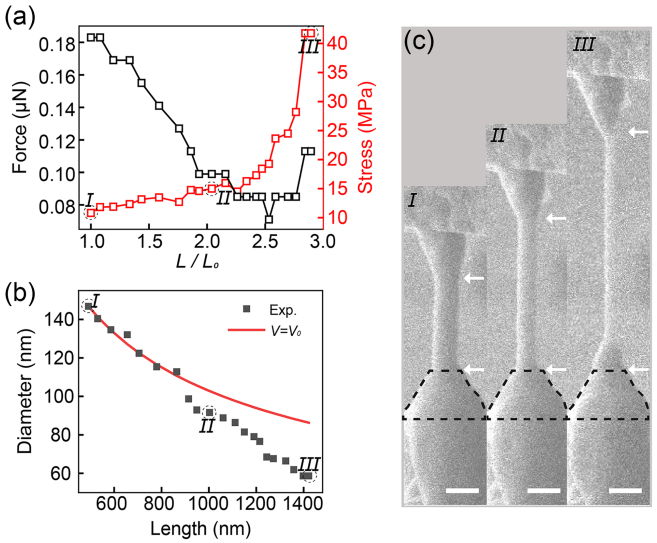


FIG. 2. *In situ* mechanical characterization of the superelongation deformation of InBiSn nanorods. (a) Typical stress-stretch ratio of an InBiSn nanorod. (b) The relationship between the diameter and the length of the InBiSn nanorod during stretching, where the black dots are the experimental data, the red line was calculated based on the constant volume assumption. (c) Snapshots of tensile testing of the InBiSn nanorod from Supplemental Material, Movie 3 [30]. Scale bar: 200 nm.

diameter ($d$) and the length ($L$) of InBiSn nanorod during uniform stretching [black dots in Fig. 2(b)]. We observed that the diameter decreases approximately linearly with the length, deviating significantly from the curve predicted from constant volume assumption (i.e., $V = V_0$), where $d = \sqrt{(4V_0/\pi L)} \propto L^{-1/2}$ [red line in Fig. 2(b)]. Further evidence supporting diffusion-based deformation is directly visualized in Fig. 2(c). By marking the shape of one end of the metal nanorod, we observed that metal atoms diffuse and accumulate near the marked region [dashed trapezoid in Fig. 2(c)].

Unambiguous evidence for pure diffusion-based deformation is also observed in the spontaneous shortening and thickening of InBiSn nanowire after tensile fracture (Supplemental Material, Figs. S2a and S3 and Movies 3 and 4 [30]). The maintained straight shape during self-shortening indicates the crystalline nature of the nanowire. Hence, we attribute the self-shortening behavior to atomic diffusion mechanism, where changes in curvature at the base of the nanowire induce a surface tension gradient, thereby driving the diffusion process. Based on the diffusion creep mechanism, the relationship between the length $L$ and time $t$ during the self-shortening process can be formulated as (see Supplemental Material [30])

$$L = \sqrt{L_0^2 - 8\frac{D_s\gamma\Omega\delta\Delta K}{kTd}t}, \tag{1}$$

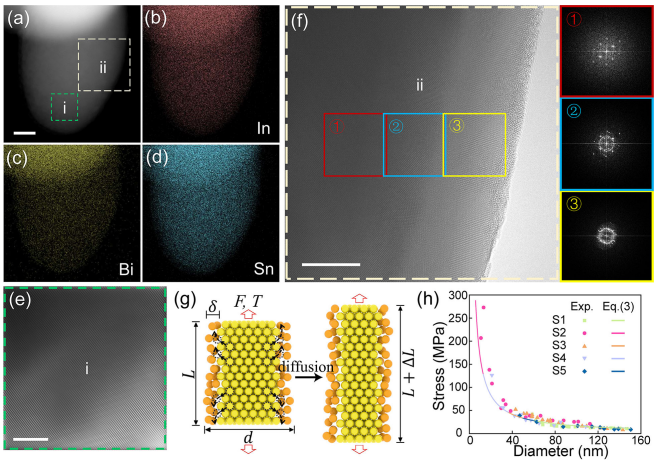


FIG. 3. TEM characterization and constitutive response of metal nanorods stretched at diffusion-based deformation temperature. (a) TEM image of an InBiSn nanorod. Scale bar: 20 nm. (b)–(d) EDS maps of the nanorod. (e) HRTEM image of the region denoted by i. Scale bar: 5 nm. (f) HRTEM characterization of the nanorod near the edge and the corresponding selected-area diffraction patterns. Scale bar: 10 nm. (g) Schematic of the atomic-scale physical process during stretching. (h) Stress versus diameter during uniform stretching, where the data points are from five independent tensile tests, the solid lines were obtained based on Eq. (3).

where $d$ is the diameter of the nanorod, $L_0$ is the length at fracture. $D_s$ is the surface diffusivity, $k$ is the Boltzmann's constant, $T$ is the absolute temperature, $\Omega$ is the atomic volume, $\gamma$ is the surface tension of the metal nanorod, and $\delta$ is the thickness of the surface layer. $\Delta K$ is the surface curvature difference of the nanorod and its basement. Equation (1) predicts that the length of nanorod would decrease faster as time, which agrees with our experimental observation (red line in Fig. S2b [30]).

Our observations provide compelling and direct experimental evidence supporting the conceptual diffusion creep mechanism in stretching metal nanorods at high homologous temperature. To characterize the microstructure of InBiSn nanorods, we molded InBiSn nanorods using nanomold with a very small cavity size (~30 nm), and then performed TEM characterization [Figs. 3(a)–3(f)]. We observed that the nanorod exhibit uniform distribution of In, Bi, and Sn elements [Figs. 3(a)–3(d)]. The high-resolution TEM (HRTEM) image also shows good crystallinity of the nanorod [Fig. 3(e)]. Notably, when enlarging the region near the edge of the nanorod, a surface amorphous layer is revealed from the selected area electron diffraction patterns [Fig. 3(f)]. We attribute this unique crystal-core–amorphous-shell structure to the approaching of melting temperature of InBiSn at room temperature (~$0.87T_m$). To further verify that the surface amorphous layer is intrinsically caused by the material whose $T_m$ is low, we irradiated an InBiSn nanorod with a 200 kV electron beam for 200 s, the interface between the crystal core and the surface amorphous layer moves toward the crystal core side, as a result, the thickness of surface amorphous layer increases from ~1.8 to ~3.6 nm [Figs. S4(a) and S4(b)]. For comparison, we also prepared Al nanorods by nanomolding bulk Al at 500 °C and in air, we observed a surface oxide layer in the Al nanorods. However, after being exposed to 200 kV electron irradiation for 200 s, the interface between the crystal core and the surface oxide layer is very stable and the thickness of the surface oxide layer is almost unchanged after irradiation [Figs. S4(c)–and S4(d)]. This is reasonable since room temperature corresponding to $0.87T_m$ of InBiSn, and $0.31T_m$ of Al, respectively, therefore, the input energy of electron irradiation can be enough to activate surface atom diffusion in InBiSn nanorods, but it is too low for Al.

To reveal the atomic-scale physical process during stretching, we applied MD simulation to mimic the tensile testing of metal nanorods near the melting temperature (see Supplemental Material [30]). As an alternative to simulating the tensile of InBiSn nanorod due to the unavailable force field, we investigated the similar behavior of stretching In nanorod near its melting temperature. A semiempirical interatomic potential specifically developed for In [32,38] was employed in the simulations. Upon equilibration of the system, we observed the presence of a surface amorphous layer enveloping a crystalline core, with the diffusivity along the surface layer at least one order of magnitude greater than that within the crystal core (Fig. S5 [30]). Throughout the tensile testing of the crystal-core–liquid-shell structure, we noted that dislocation nucleation and propagation can result in surface steps at the interface; these steps were swiftly eliminated owing to the rapid diffusion of surface atoms (see Supplemental Material, Fig. S6b and Movie 5 [30]). As a result, the nanorod is uniformly stretched.

Based on the insights gained from TEM characterization and MD simulations, specifically the presence of a surface amorphous layer encasing the crystal core, we propose a crystal-core–liquid-shell structural model for metal nanorods undergoing high-temperature elongation [Fig. 3(g)]. During the steady-state stretching process, inner atoms of the nanorod migrate toward the surface amorphous layer [solid arrows in Fig. 3(g)], where vacancies are most concentrated. They then diffuse rapidly along the amorphous layer [dashed arrows in Fig. 3(g)]. Notably, the surface diffusion within the amorphous layer is much higher compared to the lattice diffusion inside the crystal (Fig. S5 [30]). This underpins the prevailing role of lattice diffusion, represented by the Nabarro-Herring creep mechanism [3,4], in governing the constitutive response of the crystal core. Considering that the surface tension effect also becomes important at nanoscale, the equilibrium between the Nabarro-Herring creep stress, the surface tension, and the external load applied to the nanorod can be expressed as

$$F = \frac{\pi k_B T d_1^3}{4BD\Omega}\frac{dL}{dt} + \pi d\gamma, \tag{2}$$

where $d_1 = d - 2\delta$ is the diameter of the crystal core, $\delta$ denotes the thickness of the surface amorphous layer which is usually negligible by comparison with $d$. $B$ is a function of $L/d$ with its asymptotic value of $B_\infty = 12.37$ when $L \gg d$ [3,4]. Then the constitutive response of a metal nanorod with diffusion-controlled deformation can be obtained by substituting Eq. (2) into $\sigma = 4F/\pi d^2$, which reads

$$\sigma = \frac{k_B T d}{BD\Omega}\frac{dL}{dt} + \frac{4\gamma}{d} \tag{3}$$

Based on Eq. (3), the observed "rubberlike" mechanical behavior [data points in Fig. 3(h)] is well predicted by the theory [the solid lines in Fig. 3(h)]. In the calculation, $\gamma = 0.417$ N/m [39], $\Omega = \frac{4}{3}\pi r^3$ ($r = 0.161$ nm is estimated from the linear combination of the atom radius of the three constituents using the mixing rule), $k = 1.38 \times 10^{-23}$ J/K, $T = 293$ K, and $D = 5.7 \times 10^{-13}$ m$^2$/s (Fig. S5 [30]) were used. The loading velocity for the five samples refers to Table S1. Notably, the fracture stress also shows significant size effect, increasing from ~25 MPa at diameter of 59 nm to ~206 MPa for diameter of 11 nm (Fig. S7a [30]). We attribute the observed "smaller is stronger" to the surface tension effect, i.e., the second term of Eq. (3). If substituting the surface energy of InBiSn ($\gamma = 0.417$ N/m [39]) into $\sigma = 4\gamma/d$, and then subtracting the surface tension from the total stress, the contribution of lattice creep stress to the fracture stress, i.e., $[(F_{\text{fracture}}/\pi R^2) - (2\gamma/R)]/(F_{\text{fracture}}/\pi R^2)$, can be obtained (Fig. S7b [30]). It is clear that the contribution of the lattice creep stress to the fracture stress is smaller than 40% for all the tested samples and shows no obvious size dependence (Fig. S7b [30]).

Physically, the fracture of metal nanorods is determined by the competition between the displacive deformation-induced necking and surface diffusion-based smoothing (Figs. S8a and S8b) [23,40,41]. First, the propagation of dislocations through the crystal core will generate surface steps in the nanorod surface, resulting in local necking (Fig. S8a [30]). While based on the MD simulations, we observed that atom diffusion in the surface liquid layer helps to flatten the surface steps (Fig. S6 [30]), thereby maintaining the uniformly stretched state. If the timescale of displacive deformation-induced necking ($t_1$) is faster than that of surface diffusion-based smoothing ($t_2$), necking fracture occurs. The two timescales can be estimated as (see Supplemental Material for the detail [30])

$$t_1 \sim \frac{2\pi R b^2 \cos\alpha}{V_c \dot{\varepsilon}} \exp\left(-\frac{Q - \tau_m V_c}{kT}\right), \tag{4}$$

$$t_2 \sim \frac{kTL^2}{4D_s \Delta E}, \tag{5}$$

where $b$ is the magnitude of the Burgers vector, $\tau_m = (F/2\pi R^2)$ is the maximum shear stress in the crystal core, $\alpha$ is the angle between the direction of maximum shear stress and the loading direction, $\dot{\varepsilon}$ is the loading strain rate, $V_c$ is the activation volume for surface dislocation nucleation [35]. $\Delta E = \gamma\Omega\Delta K$ is the chemical potential difference caused by surface tension gradient. By equating Eqs. (4) and (5), and substituting the size of a sample at fracture in our experiments, i.e., $L = 1421$ nm, $R = 29.3$ nm, and $(dL/dt) = 15.77$ nm/s (Table S1), $b \sim 0.4$ nm [42], $Q = 0.6$ eV [35], $\alpha = 45°$, $R_s = 2R$, $\gamma = 0.417$ N/m [39], $r = 0.161$ nm, $D_s = 1.2 \times 10^{-11}$ m$^2$/s (Fig. S5 [30]), and $T = 293$ K, the activation volume can be obtained as $V_c = 52b^3$ which falls within the activation volume range for surface dislocation nucleation [35]. Similarly, the activation volume of other four tested samples can also be obtained [Fig. S9 [30] ], which agrees with the general trend of higher stress leading to lower activation volume [35].

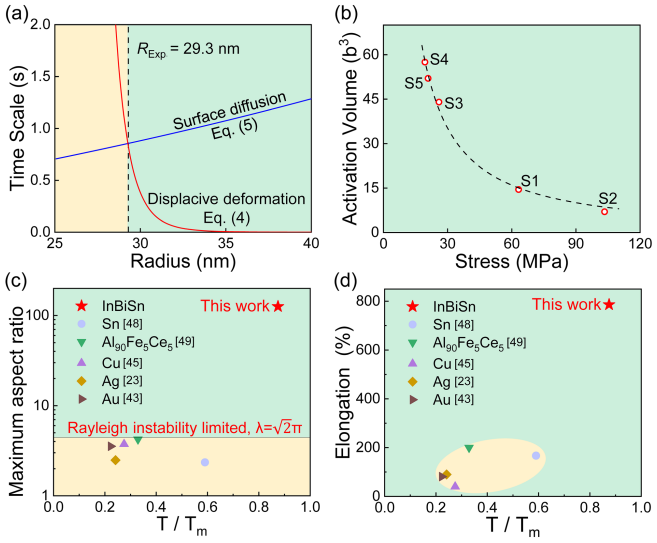


FIG. 4. (a) Comparison of the timescale of displacive deformation-induced necking and surface diffusion-induced smoothing [Eqs. (4) and (5)]. The red and blue lines represent the size-dependent timescale of displacive deformation-induced necking and the surface diffusion-induced smoothing, respectively. (b) The obtained activation volume decreases as the maximum shear stress increasing, where the black dashed line is given as a guide for the eye. (c),(d) Comparison of our experimental results with the tensile of metal nanostructures in literatures (Sn [48], $Al_{90}Fe_5Ce_5$ [49], Cu [45], Ag [23], Au [43]), where only the nanostructures with diffusion-dominated deformation mechanism were chosen for comparison. The maximum aspect ratio and elongation correspond to the values at the moment of fracture.

It is noteworthy that the enhanced surface atom diffusion at the nanoscale has been observed in the liquidlike pseudoelasticity in tensile of crystalline Ag nanoparticles [22,43], the superelongation of Ag nanorods enabled by the slip-activated surface diffusion mechanism [23], the superplasticity deformation of metal and alloy nanostructures [44], and the rubberlike deformation of Cu nanowires [45]. However, the maximum

aspect ratio of stretched nanostructures in previous studies cannot exceed $\lambda = \sqrt{2}\pi$, as limited by the Raleigh instability [46,47], and the maximum elongation is smaller than 300% [Figs. 4(a) and 4(b)]. In contrast, the maximum aspect ratio and elongation in our experiments are up to ~125 and 786%, respectively, significantly larger than previous studies [Figs. 4(a) and 4(b)]. We attribute this significant difference to the tensile of metal nanorods at high homologous temperature in our experiments, which results in the unique crystal-core–liquid-shell structure of metal nanorods as revealed by the TEM characterization [Fig. 3(f)] and MD simulations (Fig. S5 [30]).

In summary, our study provides the first compelling direct experimental evidence of the conceptual model for describing diffusion creep. Our findings shed light on the intriguing phenomenon of superelongation deformation in metal nanorods at high homologous temperatures, reaching up to approximately 0.87 times their melting temperature. Additionally, we observe a pronounced size effect on the fracture stress of these nanorods. To explain these observations, we propose a "crystal-core–liquid-shell" structure model based on the insights gained from TEM characterization and MD simulations. Furthermore, we develop a comprehensive constitutive law that incorporates diffusion creep mechanism and surface tension effect, allowing us to quantitatively predict the observed superelongation behavior and the unexpected size effect. These findings serve as a benchmark for understanding the constitutive response of nanoscale metallic crystals dominated by diffusion processes.

The authors acknowledge support from the National Natural Science Foundation of China (No. 12172260 and No. 12102307), the Fundamental Research Funds for the Central Universities (No. 2042023kf0233, No. 2042024kf0012, and No. 2042022kf1177), the starting-up fund of Wuhan University, the Large-scale Instrument and Equipment Sharing Foundation of Wuhan University. Computations were conducted at the National Supercomputer TianHe-1(A) Center in Tianjin and the Supercomputing Center of Wuhan University. We thank L. Li and Y. Zhang from the Core Facility of Wuhan University for assistance with TEM and EDS characterization.

*Corresponding author: ze.liu@whu.edu.cn
†These authors contributed equally to this work.

[1] M. D. Uchic, D. M. Dimiduk, J. N. Florando, and W. D. Nix, Science **305**, 986 (2004).
[2] D. McLean, Rep. Prog. Phys. **29**, 1 (1966).
[3] F. R. Nabarro, in *Report of a Conference on Strength of Solids* (The Physical Society, London, United Kingdom, 1948), pp. 75–90.
[4] C. Herring, J. Appl. Phys. **21**, 437 (1950).
[5] R. L. Coble, J. Appl. Phys. **34**, 1679 (1963).
[6] H. L. Duan, J. Weissmüller, and Y. Wang, J. Mech. Phys. Solids **56**, 1831 (2008).
[7] S. N. Mathaudhu, Metall. Mater. Trans. A **51**, 6020 (2020).
[8] T. Shrestha, M. Basirat, I. Charit, G. P. Potirniche, K. K. Rink, and U. Sahaym, J. Nucl. Mater. **423**, 110 (2012).
[9] S. McFadden, R. S. Mishra, R. Valiev, A. Zhilyaev, and A. Mukherjee, Nature (London) **398**, 684 (1999).
[10] L. Lu, M. Sui, and K. Lu, Science **287**, 1463 (2000).
[11] K. Sotoudeh and P. S. Bate, Acta Mater. **58**, 1909 (2010).
[12] U. D. Schwarz, Nat. Mater. **21**, 140 (2022).
[13] Y. He, D. She, Z. Liu, X. Wang, L. Zhong, C. Wang, G. Wang, and S. X. Mao, Nat. Mater. **21**, 173 (2022).
[14] T. D. B. Jacobs, C. Greiner, K. J. Wahl, and R. W. Carpick, MRS Bull. **44**, 478 (2019).
[15] J. Eggers, Phys. Rev. Lett. **80**, 2634 (1998).
[16] S. Yue, W. Yuan, Z. Deng, W. Xi, and Y. Shen, Nano Lett. **22**, 8115 (2022).
[17] M. D. Thouless, Acta Metall. Mater. **41**, 1057 (1993).
[18] T. T. Molla, J. Z. Liu, and G. B. Schaffer, Metall. Mater. Trans. B **51**, 54 (2019).
[19] Y. Chen *et al.*, Nature (London) **578**, 251 (2020).
[20] Z. Wang and B. Zhang, Energy Mater. Dev. **1**, 9370003 (2023).
[21] A. Mohiuddin, S.-i. Karato, and J. Girard, Nat. Geosci. **13**, 170 (2020).
[22] J. Sun, L. He, Y. C. Lo, T. Xu, H. Bi, L. Sun, Z. Zhang, S. X. Mao, and J. Li, Nat. Mater. **13**, 1007 (2014).
[23] L. Zhong, F. Sansoz, Y. He, C. Wang, Z. Zhang, and S. X. Mao, Nat. Mater. **16**, 439 (2017).
[24] X. Wang, S. Zheng, S. Shinzato, Z. Fang, Y. He, L. Zhong, C. Wang, S. Ogata, and S. X. Mao, Nat. Commun. **12**, 5237 (2021).
[25] D.-G. Xie, Z.-Y. Nie, S. Shinzato, Y.-Q. Yang, F.-X. Liu, S. Ogata, J. Li, E. Ma, and Z.-W. Shan, Nat. Commun. **10**, 4478 (2019).
[26] Y. Wu, Y. Zhang, L. Shui, J. Wu, and Z. Liu, Acta Mater. **225**, 117534 (2022).
[27] Z. Liu, Nat. Commun. **8**, 14910 (2017).
[28] Z. Liu, G. Han, S. Sohn, N. Liu, and J. Schroers, Phys. Rev. Lett. **122**, 036101 (2019).
[29] H. Fang, Y. Pan, C. Lu, J. Liu, T. Ding, and Z. Liu, ACS Nano **17**, 24479 (2023).
[30] See Supplemental Material at http://link.aps.org/supplemental/10.1103/PhysRevLett.132.256201 for experimental details of samples preparation and characterization, the derivation of equations, the detailed molecular dynamics simulations, supplemental Figs. S1–S9 and Table 1, which includes Refs. [1,22,27,31–35].
[31] Z. Liu, N. Liu, and J. Schroers, Prog. Mater Sci. **125**, 100891 (2022).
[32] E. C. Do, Y.-H. Shin, and B.-J. Lee, CALPHAD: Comput. Coupling Phase Diagrams Thermochem. **32**, 82 (2008).
[33] S. Plimpton, J. Comput. Phys. **117**, 1 (1995).
[34] J. R. Greer, W. C. Oliver, and W. D. Nix, Acta Mater. **53**, 1821 (2005).
[35] T. Zhu, J. Li, A. Samanta, A. Leach, and K. Gall, Phys. Rev. Lett. **100**, 025502 (2008).
[36] N. Liu, Y. Xie, G. Liu, S. Sohn, A. Raj, G. Han, B. Wu, J. J. Cha, Z. Liu, and J. Schroers, Phys. Rev. Lett. **124**, 036102 (2020).

[37] M. T. Kiani, Q. P. Sam, G. Jin, B. Pamuk, H. J. Han, J. L. Hart, J. R. Stauff, and J. J. Cha, Matter **6**, 1894 (2023).
[38] M. I. Baskes, Phys. Rev. B **46**, 2727 (1992).
[39] R. Zamora, J. Martinez-Pastor, and F. Faura, Materials **14**, 7392 (2021).
[40] Y. Wei, A. Bower, and H. Gao, J. Mech. Phys. Solids **56**, 1460 (2008).
[41] X. Li, Y. Wei, W. Yang, and H. Gao, Proc. Natl. Acad. Sci. U.S.A. **106**, 16108 (2009).
[42] L. R. Wicks and W. R. Tyson, Can. J. Phys. **53**, 1338 (1975).
[43] D. Kong *et al.*, Nano Lett. **19**, 292 (2019).
[44] P. Liu, L. Wang, Y. Yue, S. Song, X. Wang, K. M. Reddy, X. Liao, Z. Zhang, M. Chen, and X. Han, Nanoscale **11**, 8727 (2019).
[45] Y. Yue, N. Chen, X. Li, S. Zhang, Z. Zhang, M. Chen, and X. Han, Nano Lett. **13**, 3812 (2013).
[46] F. A. Nichols and W. W. Mullins, Trans. Metall. Soc. AIME **233**, 10 (1965).
[47] S. Xu, P. Li, and Y. Lu, Nano Res. **11**, 625 (2017).
[48] L. Tian, J. Li, J. Sun, E. Ma, and Z. W. Shan, Sci. Rep. **3**, 2113 (2013).
[49] J. H. Luo, F. F. Wu, J. Y. Huang, J. Q. Wang, and S. X. Mao, Phys. Rev. Lett. **104**, 215503 (2010).